Small molecule inhibitors of the SARS-CoV Nsp15 endoribonuclease

This article was published in the following Dove Press journal:
Virus Adaptation and Treatment
3 September 2010
Number of times this article has been viewed

J Ortiz-Alcantara[1]
K Bhardwaj[2]
S Palaninathan[1]
M Frieman[3]
RS Baric[3]
CC Kao[2]

[1]Department of Biochemistry and Biophysics, Texas A&M University College Station, TX, USA; [2]Department of Molecular Cellular Biochemistry, Indiana University, Bloomington IN, USA; [3]Department of Epidemiology, School of Public Health, University of North Carolina at Chapel Hill, Chapel Hill, NC, USA

Abstract: The severe acute respiratory syndrome (SARS) virus encodes several unusual RNA processing enzymes, including Nsp15, an endoribonuclease that preferentially cleaves 3' of uridylates through a ribonuclease A (RNase A)-like mechanism. Crystal structures of Nsp15 confirmed that the Nsp15 active site is structurally similar to that of RNase A. These similarities and our molecular docking analysis lead us to hypothesize that previously characterized RNase A inhibitors will also inhibit the SARS-CoV Nsp15. Benzopurpurin B, C-467929, C-473872, N-306711, N-65828, N-103019 and congo red were tested for effects on Nsp15 endoribonuclease activity. A fluorescence assay revealed that the IC_{50} values for inhibiting endoribonuclease activity were between 0.2 μM and 40 μM. These compounds were demonstrated to bind SARS-CoV Nsp15 by a differential scanning fluorimetry assay. Benzopurpurin B also inhibited the endoribonuclease activities of the Nsp15 orthologs from two other coronaviruses: mouse hepatitis virus (MHV) and infectious bronchitis virus (IBV). Benzopurpurin B, C-473872, and congo red reduced infectivity of MHV in L2 cells by 8- to 26- fold. The more effective drugs caused a decrease in MHV RNA accumulation. All three compounds reduced the infectivity of the SARS-CoV in Vero cells.

Keywords: SARS, endoribonuclease, small molecule inhibitors

Introduction

The severe acute respiratory syndrome (SARS) epidemic emerged in Southeastern China in 2002, spreading to 30 countries by 2003. It was responsible for 8096 confirmed cases with a mortality rate of about 10%. Chinese horseshoe bats are the natural reservoir of SARS-CoV-like viruses but they have been isolated also from palm civets and raccoon dogs from wild animal markets in China, suggesting that these mammals served as amplification hosts and could be the sources of infection in humans.[1–4] The existence of a natural reservoir raises the possibility of a re-emergence of SARS. The treatment used during the epidemic consisted of corticoid steroids and ribavirin although in hindsight, some of these treatments had severe side effects with minimal efficacy.[5–7] Currently there are no proven effective antiviral agents against SARS,[8] indicating the need for more specific therapeutic options.

SARS is caused by a coronavirus (SARS-CoV). It is a member of the group II Coronaviruses, which includes the mouse hepatitis virus (MHV).[9] They have a ~30 kb positive-strand RNA genome with a 5' cap and a 3' poly(A) tail. Coronaviruses are of interest in their mechanism of gene expression and replication.[1,10–12] In the early phase of infection, two large polyproteins are produced and processed by viral proteases to generate nonstructural proteins Nsp1-16, while several structural proteins

Correspondence: CC Kao
Department of Molecular Cellular Biochemistry, Indiana University, Bloomington In 47401, USA
Email ckao@indiana.edu

are translated from subgenomic RNAs.[13,14] The nonstructural proteins assemble into a membrane-associated replicase-transcriptase complex. Although the roles of many of the nonstructural proteins are not completely elucidated, it is clear that several have novel functions that are not found in positive-strand RNA viruses with smaller genomes.[9] Included in these are proteins: Nsp8, a putative RNA primase for Nsp12, the RNA-dependent RNA polymerase; Nsp14, a 3' to 5' exoribonuclease that may serve proofreading functions; Nsp15, an endoribonuclease, and Nsp16 a putative 2'-O RNA methyltransferase.[9,10,15–17] This work focuses on Nsp15, a hexameric endoribonuclease that preferentially cleaves at 3' of uridylates, forming a 2', 3'-cyclic phosphate product.[10,16,18] It has sequence and mechanistic similarities to Xendo U, which is involved in the processing of U16 small nucleolar RNAs.[19,20]

The SARS-CoV Nsp15 (herein designated sNsp15) catalytic site is formed by two His residues that act as a general base and a general acid and a Lys residue, the characteristic catalytic triad found in pancreatic RNase A.[21,22] Crystal structures of sNsp15 confirmed that the Nsp15 active site is structurally similar to that of RNase A.[21,22]

Nsp15 is a major genetic marker of nidoviruses, being absent in other RNA viruses,[16] a characteristic that makes it an ideal target for designing new antiviral therapies. The functional and structural similarities to RNase A led us to examine whether ribonuclease inhibitors can serve as lead compounds for the development of Nsp15-specific inhibitors. benzopurpurin B, C-473872, C-467929, N-306711, N-103019 and N-65828 were previously described as inhibitors binding to the active site of angiogenin (a pyrimidine specific RNase A family protein implicated in angiogenesis in tumor growth) and RNase A.[23,24] Congo red is an analog of benzopurpurin B. We demonstrate that three of these compounds affected Nsp15 enzymatic activity *in vitro* and coronavirus infection in cultured cells.

Materials and methods

Reagents

SARS and MHV Nsp15 proteins His-tagged at their N termini, and IBV Nsp15 with an His-tag at both termini were expressed in *E. coli* and purified by metal ion affinity chromatography and Mono Q ion exchange chromatography as previously described.[10] Concentrations of all proteins were quantified by absorbance at 280 nm and by comparison to known quantities of BSA. The proteins were stored in a buffer containing 50 mM Tris (pH 7.9), 300 mM NaCl, 1 mM dithiothreitol and 50% (v/v) glycerol at –20°C. Compounds N-306711, N-103019 and N-65828 were obtained from the National Cancer Institute. C-473872 and C-467929 were purchased from ChemBridge Corporation. benzopurpurin B and congo red were from Sigma-Aldrich (St. Louis, MO). All of the inhibitors except C-473872 and C-467929 were resuspended in water prior to use. C-473872 and C-467929 were dissolved in DMSO and used at a final concentration of 2% DMSO. The control reactions for assessing the effects of the inhibitors used either water or the identical concentrations of DMSO, as is appropriate.

Molecular modeling

The molecular docking program Dock 6.0[25,26] was used to execute flexible docking of the energy minimized inhibitor into the wild type sNsp15 crystal structure (PDB ID 2H85),[22] which was kept rigid. A set of spheres that represent the negative image of the binding pocket was defined within the 10Å radius of the sNsp15 catalytic-site residues H249, H234, K289, and Y342 to adopt the sphere-matching algorithm; incremental construction (anchor-and-grow method) was used to allocate the flexible conformations for the ligand. The automatic matching mode was used with twenty configurations per ligand building cycle. Interaction between the ligand and the receptor was evaluated by the grid score, a combination calculated from the van der Waals and electrostatic components, followed by visual inspection.[27,28]

Whether the inhibitor candidate could bind the MHV Nsp15 protein crystal structure (PDB ID 2GTH)[29] over sNsp15 was analyzed by superimposing the latter docked with benzopurpurin B over the former; for IBV a homology model was generated using Swiss-Model server (http://swissmodel.expasy.-org/SWISSMODEL.html) and superimposed on sNsp15 docked with benzopurpurin B. The Chimera program was used to prepare the models. (http://www.cgl.ucsf.edu/chimera/).

Endoribonuclease assays

A real-time endoribonuclease assay was performed as previously described.[18] Briefly, the assay used a substrate named rU from Integrated DNA Technologies, Inc. (Coralville, Iowa) whose fluorescence is quenched until cleavage at the uridylate. Fluorescence was monitored in a FLUOstar Optima (BMG Inc.) at excitation and emission wavelengths of 492 nm and 518 nm, respectively. In the inhibitor titration experiments to determine the biochemical IC_{50} values, the Nsp15 enzyme was present at 25 nM and the RNA substrate at 200 nM. The buffer contained 20 mM Hepes (pH 7.5),

1 mM dithiothreitol and 5 mM $MnCl_2$. Each concentration of inhibitor tested or control was performed in four independent assays to generate the mean and standard error.

A gel-based RNA cleavage assay is used to confirm endoribonuclease activity and was performed as described previously.[10] The 16-nt oligoribonucleotide substrate (GAAGCGAAACCCUAAG; Dharmacon Inc) was labeled at the 5' end with [γ-^{32}P]-ATP and T4 polynucleotide kinase. Each reaction contained 10,000 cpm radiolabeled RNA substrate at a final concentration of 1 μM and 26 nM Nsp15 in Buffer T (50 mM Tris-HCl [pH 7.5], 50 mM KCl, 1 mM dithiothreitol and 5 mM $MnCl_2$). The reactions were incubated at 30°C for 30 min and terminated by adding the gel-loading buffer containing 90% (v/v) formamide. Gel electrophoresis used 7.5 M urea, 20% (w/v) polyacrylamide gels–0.5X TBE. Radiolabeled bands were quantified using a PhosphorImager (Molecular Dynamics).

Differential scanning fluorimetry

Differential scanning fluorimetry was performed in an Eppendorf Mastercycler® EP Realplex machine.[30] Each sample was prepared in a total volume of 50 μL containing solutions of wild-type or the H234A mutant SARS-CoV Nsp15 at 2.5 μM final concentration, SYPRO orange (Molecular probes) at 2.5 X final concentration, and inhibitor in buffer T. The 96-well plate containing all of the samples was heated at a rate of 1.0°C/min, from 25 to 95°C and the fluorescence intensity was monitored continuously. The thermal denaturation curves were obtained by plotting the first derivative of fluorescence signal in response to temperature. Each sample was tested in triplicate and the results duplicated in at least two independent assays.

Plaque formation assay

MHV plaque formation assay was performed as described in Kang et al.[31] Mouse L2 cells were grown in DMEM with 10% serum in 6-well cell culture plates at 37°C and 3% CO_2 for 48 h or until 100% confluent. MHV A59 dilutions (10^{-1} to 10^{-6}) were prepared in DMEM without serum. Virus inoculum and inhibitor were incubated 15 min at 4°C. Cells were infected and incubated 1 h at room temperature then covered with 3 mL of a mixture 1:1.5 of 2X DMEM 2% serum and 1.6% agarose (equilibrated to 45°C). Plates were cultured for 48 h, stained with a 1% crystal violet solution and the number of plaques formed was used to calculate the PFU/mL. Each inhibitor was tested at 100 μM in triplicate. The same protocol was used for plaque assays of the SARS-CoV in Vero cells.

Labeling of viral RNAs

L2 cells (2.25×10^5 per well) were seeded in 12-well plates and incubated at 37°C in a CO_2 incubator for 12 h. Cells were infected with MHV at an MOI of 1 in the presence or absence of 100 μM inhibitor and incubated for 6 h, washed twice with phosphate-free DMEM, fed with DMEM supplemented with 2% dialyzed fetal bovine serum and Actinomycin D (10 μg/mL) and incubated at 37°C in CO_2 incubator. After a 15-min incubation, the medium was replaced with phosphate-free DMEM supplemented with 2% dialyzed serum, 10 μg/mL Actinomycin D and 200 μCi/mL $^{32}PO_4$. Cultures were further incubated at 37°C in CO_2 incubator for 5.5 h. The radiolabeled cultures were washed twice with ice-cold phosphate-buffered saline and RNA was extracted using an RNeasy mini kit (Qiagen Inc). Purified RNA was mixed with formaldehyde gel-loading buffer containing ethidium bromide, incubated at 65°C for 15 min, chilled on ice and loaded onto a 1% formaldehyde-agarose gel. Electrophoresis was carried out at 100 V for 6 h. Following electrophoresis, the gel was illuminated with UV light and the image was captured with a BioDoc-It imaging system, and the relative amounts of 28S rRNA bands were determined by densitometry. The gel was then fixed with 70% methanol for 30 min, dried over vacuum and exposed to a PhosphorImager screen for quantification using Molecular Dynamics software.

Results

Computational docking of RNase A and angiogenin inhibitors

Compounds active against RNase A[23] and angiogenin,[24] which have an RNase A active site, were selected for analysis against the SARS-CoV Nsp15 protein. The RNase A inhibitors are benzopurpurin B, C-473872, and C-467929 (Figure 1A). The angiogenin inhibitors are N-306711, N-103019, and N-65828 (Figure 1B).

We first used computational docking of the compounds into the structure of sNsp15 (PDB 2H85) to determine whether the compounds are sterically and electronically compatible with the active site structure of sNsp15 formed by the residues Y342, H234, H249 and K289, and/or the spaces in Nsp15 adjacent to the active site. Graphic representation of the locations for the benzopurpurin B and N-65828 are shown in Figure 1C and 1D. To provide references for the docking scores, docking experiments were performed with UTP and also glucose to yield scores of −59.4 and −27.8, respectively (Figure 1E). The docking scores for the RNase

A inhibitors (benzopurpurin, C-473872, and C-467929) were comparable to those of UTP and better than the scores for the angiogenin inhibitors (Figure 1E).

We also analyze the docking of congo red, which is chemically similar to benzopurpurin B except that it lacks the two methyl groups in the inner two of the six-member rings and assumes a slightly different conformation (Figure 1A). Congo red had a slightly better docking score (−57.8) than benzopurpurin B (−54.8) and was thus added to the compounds that we would test in functional assays. The docking results suggest that it will be useful to examine the effects of the inhibitors on Nsp15 endoribonuclease activity.

Effects of the inhibitors on sNsp15 endoribonuclease activity

A real-time fluorescence assay and highly purified recombinant sNsp15 protein were used to examine the efficacy of the inhibitors against sNsp15 *in vitro*.[18] All of the compounds showed a concentration-dependent inhibition of sNsp15 endoribonuclease activity and an examination of the output of such an assay performed with benzopurpurin B is shown in Figure 2A.

To confirm that the real time cleavage results are illustrative of inhibition of RNA cleavage activity, the effects of the compounds on the cleavage of a previously characterized 16-nt RNA in a gel-based assay was performed. The results were consistent with those from the real time assay (Figure 2B). The remainder of the results presented will be from the real-time assay. The concentration of inhibitors needed to reduce sNsp15 endoribonuclease activity by 50% and 90% (IC_{50} and IC_{90} respectively), were determined for each of the compound shown in Figure 1A. The rU and enzyme concentrations were kept constant and control experiments were performed with either aqueous buffer or buffer amended with DMSO to take into account the use of DMSO to solubilize some of the compounds. Inhibitor titration experiments with benzopurpurin B and congo red are shown in Figure 2C and a summary of all of the IC_{50} and IC_{90}s are shown in Figure 2D. benzopurpurin B was the best biochemical inhibitor of the seven, with IC_{50} and IC_{90} of 0.2 and 0.9 μM, respectively. Consistent with the trends in the docking scores, compounds developed against RNase A were more effective Nsp15 endoribonuclease inhibitors than those developed against angiotensin. However, the relative ranking of the results from two assays did not correspond.

Select inhibitors can bind Nsp15

To demonstrate that the compounds could bind to the sNsp15, we examined for changes in Nsp15 using a differential scanning fluorimetry (DSF) assay. The assay detects changes in the fluorescence of the dye SYPRO orange, which fluoresces better upon binding to the hydrophobic regions of a protein that are exposed by increasing temperature. The transition curves are complex, as would be expected by the unfolding of an oligomeric protein, however, a major peak could be readily identified (Figure 3). The temperature where there

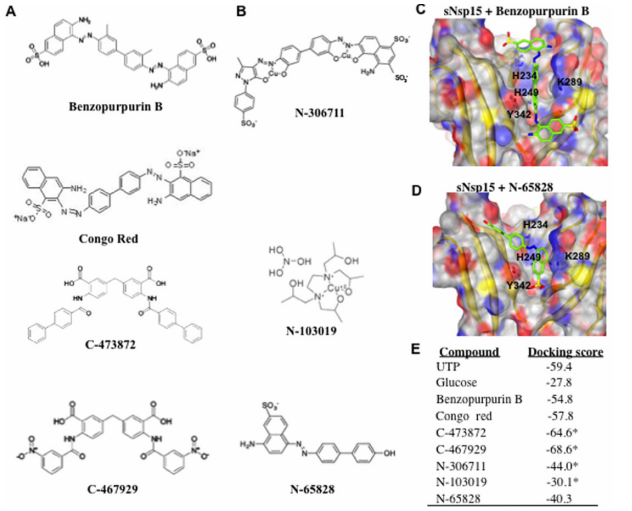

Figure 1 Small-molecule inhibitors assayed for effects on Nsp15. **A**) Inhibitors of RNase A previously reported by Jenkins and Shapiro.[23] Congo red was also tested since it is a benzopurpurin B analog. **B**) Inhibitors of angiogenin previously reported by Kao et al.[24] **C**) The docking of benzopurpurin B to the catalytic site of sNsp15. The docking conformation with the highest score is shown. The C-terminal active site groove is shown in a yellow ribbon representation under a semi transparent surface colored by atom. The catalytic site residues are labeled. The inhibitor stacks with Y342 residue and occupies the entire C-terminal active site groove of SARS-CoV Nsp15. **D**) The docking conformation of N-65828 in the sNsp15 catalytic site. **E**) The docking score of each tested inhibitor.

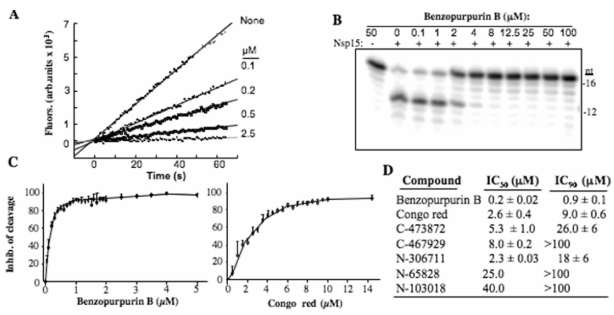

Figure 2 Effects of the small molecule inhibitors on the SARS-CoV Nsp15 endoribonuclease activity. **A**) Representative results of a real-time endoribonuclease assay showing the inhibitory effect of different concentrations of benzopurpurin B on the SARS-Nsp15 activity. The slope of the change in fluorescence was used to determine the rate of cleavage by Nsp15. **B**) A demonstration of the results from a gel-based RNA cleavage assay. This assay was performed in presence of increasing concentrations of benzopurpurin B. **C**) Benzopurpurin B and congo red titration plots using the real-time endoribonuclease assay showing concentration dependent inhibition of the substrate cleavage by sNsp15. **D**) A summary of the IC_{50} and IC_{90} values for the small-molecule compounds tested on SARS-Nsp15.

is a maximal transition in this peak will be designated the Tm^{App}. All samples were tested in triplicate and in a buffer capable of supporting enzymatic activity that included 5 mM Mn^{2+}, which we observed to help in smoothing the changes in transition, likely by affecting sNsp15 conformation, as previously demonstrated by Bhardwaj et al.[10] A reaction performed in the absence of sNsp15, but in the presence of these concentrations of benzopurpurin B or other inhibitors tested did not change the fluorescence of SYPRO orange. The denaturation profiles changed in a concentration-dependent manner for all of the compounds tested (Figure 3A, upper panels and data not shown). These results provide qualitative data for the compounds binding to Nsp15.

Given that the inhibitors were originally active site inhibitors of RNase A and angiogenin, it is likely that they will act as competitive inhibitors of sNsp15. To confirm that the inhibitors act at the active site, we examined whether Nsp15 with an active site substitution, H234A, would exhibit the changes in the denaturation profile in the differential scanning fluorimetry assay. Congo red and C-473872 were tested. With the WT Nsp15, the presence of both compounds resulted in obvious shifts in the fluorescence profile exhibited by SYPRO orange as a function of temperature (Figure 3A, two upper panels). With the H234A mutant, we observed that its profile was significantly shifted to a lower temperature even in the absence of inhibitor, but Nsp15 can exist in an equilibrium as a monomer, trimer and a hexamer in a concentration-dependent manner.[32] However, the presence of C-473872 or congo red caused only minor changes in the denaturation profile of the protein as seen with wild-type Nsp15 (Figure 3, lower two panels). These results are consistent with the inhibitors interacting with Nsp15 through the active site.

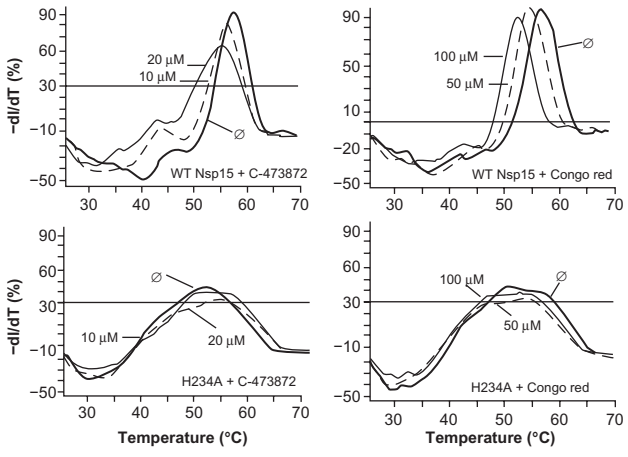

Figure 3 Select inhibitors can bind Nsp15. Analysis of the binding between the SARS-CoV Nsp15 protein and select inhibitors using differential scanning fluorimetry. The graphs show the first derivative of the differential scanning fluorimetry assays for wild-type sNsp15 and a protein with a substitution in the catalytic pocket H234A. The point of maximal change in the fluorescence of the dye SYPRO orange can be taken as the apparent Tm.

The MHV and IBV Nsp15 are also sensitive to benzopurpurin B *in vitro*

Coronaviruses can be important pathogens of animals as well as humans.[9,11,34] Elucidation of the structure of the mouse hepatitis virus Nsp15 (mNsp15) and molecular modeling revealed that the active site structure is highly similar to that of the SARS-CoV Nsp15.[29,32] We wanted to determine whether an inhibitor active against the SARS-CoV Nsp15 will have similar effects on the Nsp15 proteins of other coronaviruses. Superimposition of sNsp15 docked with benzopurpurin B on top of mNsp15 showed that benzopurpurin B-like inhibitors could be accommodated within the MHV Nsp15 active site (Figure 4A). When tested for effects on RNA cleavage by the MHV Nsp15 protein expressed in *E. coli*, benzopurpurin B was found to have an IC_{50} and IC_{90} of 0.4 and 0.9 μM, highly similar to the values obtained with the SARS-CoV Nsp15 (Figure 4B).

To extend the analysis further, we tested the effects of benzopurpurin B on the Nsp15 of infectious bronchitis virus (IBV, to be named iNsp15), which was demonstrated by Bhardwaj et al[10] to also cleave uridylates. Since the iNsp15 structure has not been determined, we threaded its sequence into the crystal structure of the SARS-CoV. The active site of the protein was essentially comparable to that of the SARS-CoV and MHV orthologs and could accommodate benzopurpurin B (Figure 4C). A prediction of this analysis is that the iNsp15 will also be inhibited by the compounds effective on the MHV and SARS-CoV Nsp15. Indeed, iNsp15 was inhibited by benzopurpurin B in a concentration-dependent manner and with IC_{50} and IC_{90} values similar to that of the MHV and SARS-CoV Nsp15 enzymes (Figure 4D). These results suggest that the Nsp15 orthologs from these three Coronaviruses likely have highly similar active site pockets. Furthermore, it should be possible to use model coronaviruses to study the effects of these drugs on viral infection under conditions that do not require BSL3 containment.

Inhibition of MHV infection in cell culture

The effect of the compounds on MHV replication was investigated in plaque formation assays using mouse L2 cells. The cells were plated in six-well cell culture plates and grown until 100% confluence then infected with different dilutions of MHV A59 and the inhibitor at a final concentration of

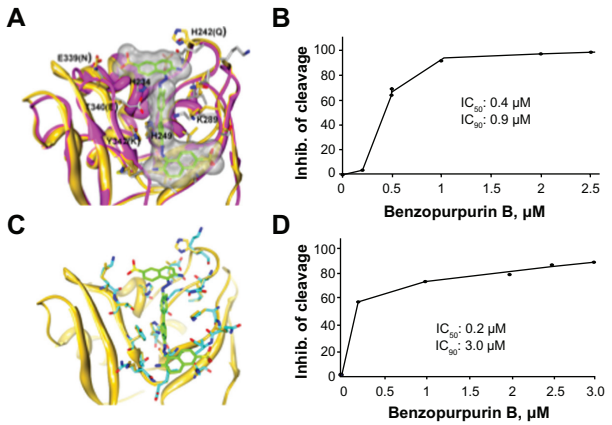

Figure 4 Benzopurpurin B inhibition of the *in vitro* RNA cleavage by other Coronavirus Nsp15 orthologs. **A**) A model for the binding of benzopurpurin in the MHV Nsp15 crystal structure (magenta ribbon and grey sticks; PDB ID 2gth). Although the catalytic site residues are identical, the nearby residues are not conserved between sNsp15 and mNsp15 (non-conserved residues are shown in parenthesis). Perhaps the flexibility of the C-terminal active site residues should enable the inhibitor binding to mNsp15 as well. **B**) Effects of benzopurpurin B on the MHV Nsp15 ortholog. The enzyme is inhibited in a concentration dependent manner. **C**) A model of the IBV Nsp15 ortholog. The active site residues in the IBV NSp15 homology model are well conserved with the SARS-Nsp15. **D**) Effects of benzopurpurin B on endoribonuclease activity of the IBV Nsp15 ortholog using the real time fluorescent assay.

100 μM. After a 1-h period to allow the infection to initiate, the cells were covered with a mixture of medium and agarose. After a two-day incubation, the plaques were stained and counted. In three independent experiments, congo red reproducibly showed the most inhibition of MHV plaque formation, with the mean reduction of plaque formation being 27-fold. Compound C-473872 caused a 10-fold reduction, and benzopurpurin B, despite being the best inhibitor in the biochemical assay, resulted in only an 8-fold reduction in PFUs. None of the compounds had an obvious effect on the shape or viability of the cells when present at 100 μM (Figure 5A and B and data not shown).

To confirm and extend the analysis of the compounds on MHV infection, we examined MHV RNA production in the presence of benzopurpurin B, congo red, and C-473872. Genomic and subgenomic RNAs were reduced in the presence of the drugs, with C-473872 being the most effective and benzopurpurin B having only a minimal effect in cells. Furthermore, both the genomic and subgenomic MHV RNA levels were uniformly affected (Figure 5C).

Effect on SARS-CoV in cultured Vero cells

To examine whether the compounds could inhibit the SARS-CoV in cells, plaque assays were performed in Vero cells using a 100 μM final concentration of several inhibitors. Again, no obvious differences in cell growth or morphologies were observed under the conditions used. However, the inhibitory effects, while reproducible, were less than those observed with MHV infected L2 cells. Consistent with the MHV results, the relative degree of effectiveness of congo red, C-473872, and benzopurpurin B were also observed in Vero cells (Figure 6). Congo red caused a 4.3 fold decrease in plaque formation at 100 μM (Figure 6). At 500 μM congo red, a ca. 10-fold decrease was observed (Frieman, data not shown). Unlike the results with MHV, N-306711 did exhibit some inhibition of SARS-CoV plaque formation in Vero cells.

Discussion

There is currently a need to develop both vaccines and antivirals against coronavirus infections. The Nsp15 endoribonuclease is a diagnostic for coronaviruses and is an unusual enzyme for RNA viruses. We took advantage of the observation that Nsp15 has an RNase A-like active site and a mechanism for RNA cleavage identical to RNase A to test previously identified inhibitors of RNase A and angiogenin.[17,21–24]

Computational docking into the structure of sNsp15 predicted that small-molecule inhibitors of angiogenin and RNase A could bind to the Nsp15 active site (Figure 1). Functionally, three angiogenin and RNase A inhibitors, C-473872, C-467929, benzopurpurin B, and the structurally related congo red, were found to be potent inhibitors of the sNsp15 endoribonuclease activity *in vitro*. To put this into context, we have tested more than 50 candidates that had high probability of docking into the sNsp15 active site and found no compounds that had IC_{50} values better than 50 μM (Bhardwaj et al unpublished data). Obtaining four inhibitors out of seven with IC_{50}s of better than 10 μM is thus a pleasant surprise. The results add a layer of functional relevance to the claims that sNsp15 has an RNase A-like catalytic pocket and cleavage mechanism for the Nsp15 of different coronaviruses.[21,22]

The three characterized compounds acted as competitive inhibitors and affected RNA cleavage. Benzopurpurin B, congo red, and C-473872 were able to bind sNsp15 since they induce a concentration-dependent shift of the Tm of sNsp15. Benzopurpurin B and C-473872 induce an increase in the sNsp15 Tm that corresponds to a stabilizing effect of the compounds. Since benzopurpurin B and C-473872 are active site inhibitors,[23,24] and congo red is likely to be one as well, it is logical to assume that these compounds are competitive inhibitors. Consistent with this, a mutation in the catalytic pocket, H234 altered the spectroscopic properties of the sNsp15 in the presence of congo red or C-473872. We note that the mutant protein has a spectroscopic profile distinct

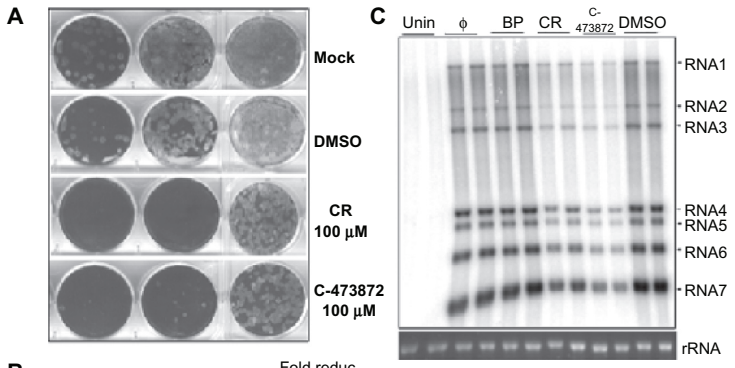

B

Compound. conc.	P(u/mL)	Fold reduc. (N = 3)
Mock	1.8×10^7	
Benzopurpurin B, 100 μM	2.2×10^6	8.2 ± 0.2
Congo red, 100 μM	6.6×10^5	27.2 ± 0.3
Mock	4.9×10^5	
C-473872, 100 μM	4.9×10^5	10.0 ± 2
C-467929, 100 μM	3.0×10^5	1.6 ± 3
N-306711, 100 μM	8.5×10^5	none

Figure 5 Effects of select Nsp15 inhibitors on MHV plaque formation in mouse L2 cells. **A**) Representative plaque assay results in presence of congo red and C-473872 at 100 μM, or controls such as the solvent DMSO. **B**) A Summary of the effect of the small-molecule compounds on MHV replication in L2 cells. The number of PFU/mL obtained and the fold reduction observed in three independent assays are reported. The compounds were tested in two sets and the mock from each was used to normalize the effects of the compounds as fold reduction in MHV plaque formation. **C**) Effects of the compounds on MHV RNA accumulation. The RNAs shown in the gel image are the MHV A59 RNA expressed in L2 cells 12 h after the addition of the virus. The compounds shown above the gel image were added to the cells at 100 μM final concentration at the time of virus addition. Five hours later, the medium was replaced with the ^{32}P-containing medium lacking the compounds for an additional 7 h. The RNAs were processed as described by Kang et al.[31] The identities of the RNAs are shown to the left of the gel image. The rRNAs was taken from the ethidium bromide-stained gel used for autoradiography. It is intended to serve as a loading control.

from the wild-type Nsp15. At this point, we do not understand the reason for this change and can only speculate that the C-terminus of Nsp15 helps to form the fairly dynamic active site[21,22] and that the active site residues may contribute to the stability of the Nsp15 hexamer. While binding at the active site is entirely consistent with all results so far, we cannot presently rule out additional binding sites for these compounds in sNsp15.

Importantly, congo red and C-473872 reduced the infection of MHV and the SARS-CoV in cultured cells by approximately a log. We note with interest that mutations in the active site of the MHV Nsp15 also caused only a one to two-log decrease in viral titers.[31] A one log decrease titer in virus production and/or viral ligands could have a significant effect in the outcome of infection and on the induction of immune responses.[34,35]

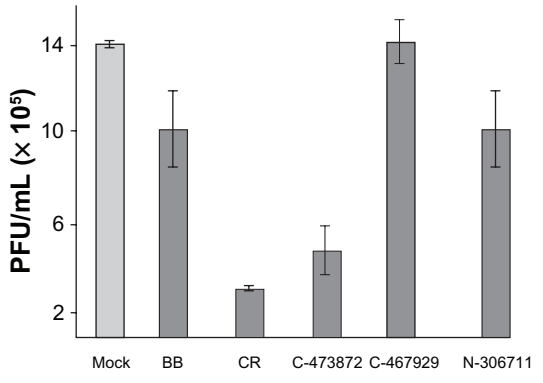

Figure 6 Effect of the small-molecule compounds on SARS-CoV infection on Vero cells. The plots illustrated a reduction in the number of plaque forming units in the presence of the compounds at 100 μM. BB: benzopurpurin B.

The compounds should be considered as the first generation hits. The effective concentrations in cell-based assays need to be improved at least one to two logs before these compounds can be considered useful as antivirals. The discrepancy between the biochemical results (IC_{50}s in the low micromolar range) and the effective concentrations in cells is likely to be, in a large part, due to the pharmacological properties of the compounds, features that we have not pursued in this work. Notably, the fact that benzopurpurin B differed from congo red only by the presence of two methyl groups indicates that small modifications to congo red or benzopurpurin B could have dramatic effects on the efficacy of these compounds in cells.

Congo red is also a compound used in the imaging and treatment for amyloid plaques.[25,36] It can also interact with other nucleotide-binding enzymes,[37] thus accounting for its efficacy for RNase A and Nsp15. Treatment of hamsters with congo red and its derivatives were shown to maximally delay the onset in Scrapies when it was administered to the animals,[38,39] indicating that it is possible to use congo red in infected animals. However, congo red does not readily cross the blood-brain barrier and there is potential cytotoxicity due to cross-reactions to cellular enzymes.[40] Thus, a number of derivatives of congo red with altered pharmacokinetic

properties have been generated and characterized for activities in cells. It may be of interest to test these compounds for efficacy as well as desired pharmacological properties for treatments of coronavirus infection.

The compounds can also serve as new tools to analyze coronavirus infection. A proposed role for Nsp15 is that it may participate in the processing of the RNAs needed to form coronavirus subgenomic RNAs.[9] However, there is no direct evidence for this in MHV. In fact, mutational analysis of the mNsp15 resulted in a general decrease in all MHV RNAs and an approximately one log decrease in MHV virion production. If Nsp15 does have a direct effect on subgenomic RNA, the effects are sufficiently pleiotropic to affect all MHV RNAs (Figure 5C).[31] The effects of the inhibitors on MHV RNA production are consistent with those from previous mutational analyses.[31] More judicious application of Nsp15 inhibitors at different stages of coronavirus infection in cultured cells could allow better insight into how Nsp15 contributes to coronavirus infection.

Acknowledgments

This research was supported in part by the National Institute of Allergy and Infectious Diseases grants 1R56AI06164 to CK, and AI059443 to RSB; JOA gratefully acknowledges a National Science Foundation enrichment supplemental grant to develop the differential fluorimetry assay; and JCS acknowledges funds from the Robert A Welch Foundation.

We thank our colleagues at Texas A&M University, especially Julian Leibowitz for advice on MHV and Thomas Ioerger, and Will Snee for many helpful discussions.

Disclosure

The authors report no conflicts of interest in this work.

References

1. Guan Y, Zheng BJ, He YQ, et al. Isolation and characterization of viruses related to the SARS coronavirus from animals in Southern China. *Science.* 2003;302:276–278.
2. Li W, Shi Z, Yu M, et al. Bats are natural reservoirs of SARS-like coronaviruses. *Science*. 2005;310:676–679.
3. Song HD, Tu CC, Zhang GW, et al. Cross-host evolution of severe acute respiratory syndrome coronavirus in palm civet and human. *Proc Natl Acad Sci U S A*. 2005;102:2430–2435.
4. World Health Organization. 2003 Aug 15, posting date. Summary table of SARS cases by country, 2002 Nov 1–2003 Aug 7.
5. Christian MD, Poutanen SM, Loutfy MR, Muller MP, Low DE. Severe acute respiratory syndrome. *Clin Infect Dis*. 2004;38:1420–1427.
6. Peiris JS, Yuen KY, Osterhaus AD, Stohr K. The severe acute respiratory syndrome. *N Engl J Med*. 2003;349:2431–2441.
7. Poutanen SM, Low DE, Henry B, et al. Identification of severe acute respiratory syndrome in Canada. *N Engl J Med*. 2003;348:1995–2005.
8. Cheng VC, Lau SK, Woo PC, Yuen KY. Severe acute respiratory syndrome coronavirus as an agent of emerging and reemerging infection. *Clin Microbiol Rev*. 2007;20:660–694.
9. Snijder EJ, Bredenbeek PJ, Dobbe JC, et al. Unique and conserved features of genome and proteome of SARS-coronavirus, an early split-off from the coronavirus group 2 lineage. *J Mol Biol*. 2003;331: 991–1004.
10. Bhardwaj K, Guarino L, Kao CC. The severe acute respiratory syndrome coronavirus Nsp15 protein is an endoribonuclease that prefers manganese as a cofactor. *J Virol*. 2004;78:12218–12224.
11. Masters PS. The molecular biology of coronaviruses. *Adv Virus Res*. 2006;66:193–292.
12. Spaan W, Cavanagh D, Horzinek MC. Coronaviruses: structure and genome expression. *J Gen Virol*. 1988;69:2939–2952.
13. Ziebuhr J. Molecular biology of severe acute respiratory syndrome coronavirus. *Curr Opin Microbiol*. 2004;7:412–419.
14. Ziebuhr J, Snijder EJ, Gorbalenya AE. Virus-encoded proteinases and proteolytic processing in the Nidovirales. *J Gen Virol*. 2000;81: 853–879.
15. Imbert I, Guillemot JC, Bourhis JM, et al. A second, non-canonical RNA-dependent RNA polymerase in SARS coronavirus. *EMBO J*. 2006;25:4933–4942.
16. Bayer V, Thiel A, Gorbalenya E, Ziebuhr J. Major genetic marker of nidoviruses encodes a replicative endoribonuclease. *Proc Natl Acad Sci U S A*. 2004;101:12694–12699.
17. Minskaia E, Hertzig T, Gorbalenya AE, Campanacci V, Canard CB, Ziebuhr J. Discovery of an RNA virus 3'->5' exoribonuclease that is critically involved in coronavirus RNA synthesis. *Proc Natl Acad Sci U S A*. 2006;103:5108–5113.
18. Bhardwaj K, Sun J, Holzenburg A, Guarino LA, Kao CC. RNA recognition and cleavage by the SARS coronavirus endoribonuclease. *J Mol Biol*. 2006;361:243–256
19. Caffarelli E, Maggi L, Fatica A, Jiricny J, Bozzoni I. A novel Mn^{++}-dependent ribonuclease that functions in U16 SnoRNA processing in *X* laevis. *Biochem Biophys Res Commun*. 1997;233: 514–517.
20. Laneve P, Altieri F, Fiori ME, Scaloni A, Bozzoni I, Caffarelli E. Purification, cloning, and of XendoU, a novel endoribonuclease involved in processing of intron-encoded small nucleolar RNAs in *Xenopus laevis*. *J Biol Chem*. 2003;278:13026–13032.
21. Bhardwaj K, Palaninathan S, Alcantara JM, et al. Structural and functional analyses of the severe acute respiratory syndrome coronavirus endoribonuclease Nsp15. *J Biol Chem*. 2008;283:3655–3664.
22. Ricagno S., M. P. Egloff, R. Ulferts, B. Coutard, D. Nurizzo, V. Campanacci, C., J. Ziebuhr, and B. Canard. 2006. Crystal structure and mechanistic determinants of SARS coronavirus nonstructural protein 15 define an endoribonuclease family. Proc. Natl Acad. Sci. USA 103:11892–11897.
23. Jenkins JL, Shapiro R. Identification of small-molecule inhibitors of human angiogenin and characterization of their binding interactions guided by computational docking. *Biochemistry*. 2003;42:6674–6687.
24. Kao RY, Jenkins JL, Olson KA, Key ME, Fett JW, Shapiro R. A small-molecule inhibitor of the ribonucleolytic activity of human angiogenin that possesses antitumor activity. *Proc Natl Acad Sci U S A*. 2002;99:10066–10071.
25. Furumoto S, Okamura N, Iwata R, Yanai K, Arai H, Kudo Y. Recent advances in the development of amyloid imaging agents. *Curr Top Med Chem*. 2007;7:1773–1789.
26. Moustakas DT, Lang PT, Pegg S, et al. Development and validation of a modular, extensible docking program: DOCK 5. *J Comput Aided Mol Des*. 2006;20:601–619.
27. Meng EC, Shoichet BK, Kuntz ID. Automated docking with grid-based energy evaluation. *J Comp Chem*. 1992;13:505–524.
28. Shoichet BK, Bodian DL, Kuntz ID. Molecular docking using shape descriptors. *J Comp Chem*. 1992;13:380–397.

29. Xu X, Zhai Y, Sun F, et al. New antiviral target revealed by the hexameric structure of mouse hepatitis virus nonstructural protein nsp15. *J Virol*. 2006;80:7909–7917.
30. Niesen FH, Berglund H, Vedadi M. The use of differential scanning fluorimetry to detect ligand interactions that promote protein stability. *Nat Protoc*. 2007;2:2212–2221.
31. Kang H, Bhardwaj K, Li Y, et al. Biochemical and genetic analyses of murine hepatitis virus Nsp15 endoribonuclease. *J Virol*. 2007;81: 13587–13597.
32. Guarino LA, Bhardwaj K, Dong W, Sun J, Holzenburg A, Kao C. Mutational analysis of the SARS virus endoribonuclease: identification of residues affecting hexamer formation. *J Mol Biol*. 2005;353:1106–1117.
33. Lai MM, Cavanagh D. The molecular biology of coronaviruses. *Adv Virus Res*. 1997;48:1–100.
34. Kato H, Takeuchi O, Sato S, et al. Differential roles of MDA5 and RIG-I helicases in the recognition of RNA viruses. *Nature*. 2006;441: 101–105.
35. Yasui F, Kai C, Kitabatake M, et al. Prior immunization with severe acute respiratory syndrome (SARS)-associated coronavirus (SARS-CoV) nucleocapsid protein causes severe pneumonia in mice infected with SARS-CoV. *J Immunol*. 2008;181:6337–6348.
36. Webb S, Lekishvili T, Loeschner C, et al. Mechanistic insights into the cure of prion disease by novel anti-prion compounds. *J Virol*. 2007;81: 10729–10741.
37. Edwards RA, Woody RW. Studies of Cibacron Blue and congo red bound to dehydrogenases and kinases. Evaluation of dyes as probes of the dinucleotide fold. *Biochemistry*. 1979;18:5197–5204.
38. Ingrosso L, Ladogana A, Pocchiari M. Congo red prolongs the incubation period in Scrapie-infected hamsters. *J Virol*. 1995;69:506–508.
39. Poli G, Martino PA, Villa S, et al. Evaluation of antiprion activity of congo red and its derivatives in experimentally infected hamsters. *Arzneimittel forschung*. 2004;54:406–415.
40. Rudyk H, Vasiljevic S, Hennion RM, Birkett CR, Hope J, Gilbert IH. Screening congo red and its analogues for their ability to prevent the formation of PrP-res in scrapie-infected cells. *J Gen Virol*. 2000;81: 1155–1164.